Smart Sensing Skin for Detection and Localization of Fatigue Cracks

Sari Kharroub[1], Simon Laflamme[1,2], Chunhui Song[1], Daji Qiao[2], Brent Phares[4], Jian Li[5]

[1]Department of Civil, Construction, and Environmental Engineering, Iowa State University, Ames, IA, 50011, USA
[2]Department of Electrical and Computer Engineering, Iowa State University, Ames, IA, 50011, USA
[3]Bridge Engineering Center, Institute for Transportation, Iowa State University, Ames, IA, 50011, USA
[4]Department of Civil, Environmental and Architectural Engineering, The University of Kansas, Lawrence, KS, 66045, USA

E-mail: laflamme@iastate.edu

PACS numbers: 46.50.+a, 07.07.Df,07.07.Mp,07.10.Pz,81.70.Bt,89.20kk

Submitted to: *SMS*

Abstract. Fatigue cracks on steel components may have strong consequences on the structure's serviceability and strength. Their detection and localization is a difficult task. Existing technologies enabling structural health monitoring have a complex link signal-to-damage or have economic barriers impeding large-scale deployment. A solution is to develop sensing methods that are inexpensive, scalable, with signals that can directly relate to damage. The authors have recently proposed a smart sensing skin for structural health monitoring applications to mesosystems. The sensor is a thin film soft elastomeric capacitor (SEC) that transduces strain into a measurable change in capacitance. Arranged in a network configuration, the SEC would have the capacity to detect and localize damage by detecting local deformation over a global surface, analogous to biological skin. In this paper, the performance of the SEC at detecting and localizing fatigue cracks in steel structures is investigated. Fatigue cracks are induced in steel specimens equipped with SECs, and data measured continuously. Test results show that the fatigue crack can be detected at an early stage. The smallest detectable crack length and width are 27.2 mm and 0.254 mm, respectively, and the average detectable crack length and width are 29.8 mm and 0.432 mm, respectively. Results also show that, when used in a network configuration, only the sensor located over the formed fatigue crack detect the damage, thus validating the capacity of the SEC at damage localization.

1. Introduction

Steel structures can be subjected to substantial damage under high levels of long-term continuous loading. In the case of steel bridges, the cyclic loads imposed by heavy truck traffic or natural hazards may initiate fatigue cracks at various locations that could limit their load-carrying capacity and service life, or in the worst case provoke structural failure. Most commonly, fatigue cracks originate in the welded details of the structure. These cracks can further propagate into other components, leading to significantly expensive repairs or replacements [1]. As a result, it is critical for bridge owners to have the tools to detect and monitor fatigue cracks to improve structural safety and enable timely repairs.

The vast majority of fatigue crack detection is conducted using visual inspections, which are expensive and may fail at detecting existing fatigue cracks if they are not directly observable. Non-destructive evaluation (NDE) techniques are also being used. They have the potential to detect unobservable fatigue cracks and monitor their development. They include acoustic emission [2, 3, 4], ultrasonic waves [5], eddy current [6, 7], thermography [8], and vibrothermography [9]. However, NDE methods have limited real-time applicability and are also expensive to perform.

Structural health monitoring (SHM) is the automation of the inspection process. Unlike NDE techniques, SHM technologies can typically be applied continuously, in real time. However, most of SHM technologies have a complex link signal-to-damage, which limits the capability to detect and localize damages. Recent literature includes several SHM technologies developed for crack monitoring. Zhang [10] proposed a polymer-based

piezoelectric paint sensor to detect surface cracks. The paint is deployed onto the desired surface and a signal is generated upon mechanical strain. Electromechanical impedance-based methods have also been studied and applied. For instance, Yu et al. [11] used a piezoelectric wafer active sensors (PWAS) network for monitoring of steel bridges, with the potential to detect and localize damage, and Gresil et al. [12] experimentally investigated the utilization of PWAS for monitoring of fatigue crack growth in a thick steel plate. Ihn et al. [13] and Gama et al. [14] used piezoelectric sensors to detect hidden fatigue crack growth. While being promising at monitoring fatigue cracks, piezoelectric technologies typically have high impedance and may be sensitive to the quality of the surface bond. Tsuda et al. [15, 16] proposed a combined SHM system comprising a fiber Bragg grating sensor and a piezoelectric transmitter to monitor fatigue crack propagation in stainless steel. Lee et al. [17] proposed to monitor fatigue damage using embedded intensity-based optical fiber (IBOF) sensors. Optical sensors have the advantage to withstand corrosive environment and they have immunity to electromagnetic interference [18], but can be brittle and expensive to measure. Other sensors employed in fatigue crack detection include passive wireless antenna sensor [19, 20], eddy current sensors [21], and vacuum crack sensors [22].

The authors have recently proposed a soft elastomeric capacitor (SEC) for monitoring of strain over large surfaces [23, 24]. The sensing principle is based on measuring a change in the sensor capacitance that follows a change in its geometry (i.e., strain). Arranged in a network configuration, this skin-type sensor has the potential to detect and localize fatigue cracks on a surface. Others have proposed such skin-type sensors [25, 26, 27, 28, 29, 30]. In particular, capacitive-based technologies include applications to humidity, pressure, strain, and tri-axial measurements [31, 32, 33, 34, 35].

The SEC technology would be an alternative to resistive strain gauges to easily cover large surfaces, at low cost. In prior work, the authors have demonstrated that the sensor can be used as a strain gauge with a resolution of 25 $\mu\varepsilon$ [24] and as a dynamic vibration sensor [36, 37]. In this paper, the potential of the sensing solution at detecting and localizing fatigue cracks in steel is investigated. The objective is to understand the behavior of the sensor under small and localized strains, and guide future developments for deploying large sheets of SECs onto steel structures for fatigue crack monitoring.

The paper is organized as follows. Section 2 presents fabrication process of the SEC, derives its electromechanical model, and validates its sensing principle. Section 3 describes the methodology used to detect fatigue cracks accompanied by the experimental results. Section 4 presents of results for fatigue crack detection and localization. Section 5 concludes the paper.

2. Smart Sensing Skin

2.1. Sensor Fabrication

The dielectric of the SEC is composed of a poly(styrene-*block*-ethylene-*co*-butylene-*block*-styrene) (SEBS) matrix filled with titania (TiO_2). SEBS is a block copolymer widely used for medical applications, because of its purity, softness, elasticity, and strength [38]. Titania is an inorganic particle characterized by a high dielectric permittivity that increases the permittivity and durability of the SEBS matrix [39]. The dielectric is sandwiched between two electrodes. They are constituted from the same organic matrix, but filled with carbon black (CB) particles to create a conductive polymer. These CB particles are selected to improve conductivity at low cost, and prolong the life time of the polymer due to their antioxidant and ultraviolet light stabilization properties [40]. The utilization of the same polymer matrix (SEBS) for both the electrodes and dielectric results in a strong mechanical bond between the layers that constitute the SEC. The SEC is fabricated using a solution cast process, shown in Fig. 1, as follows:

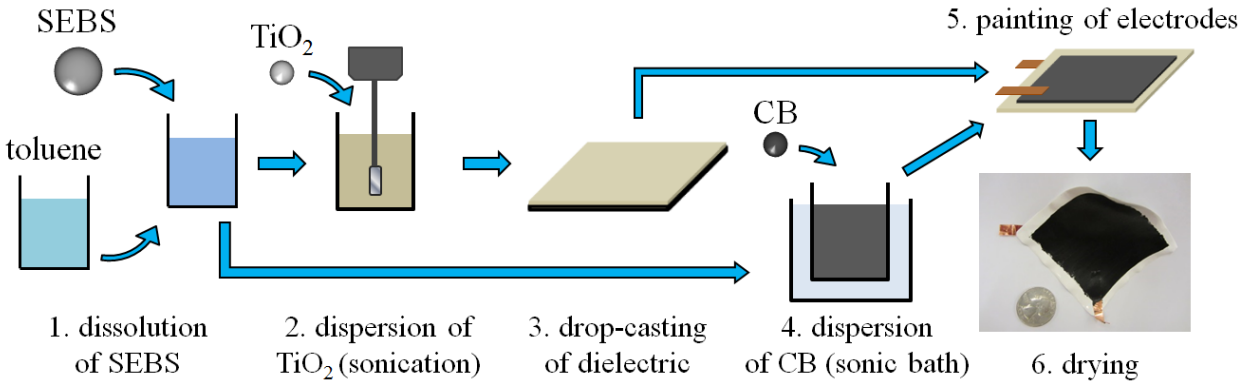

Figure 1: Fabrication process of the SEC.

(i) SEBS (Mediprene Dryflex) particles are dissolved in toluene.

(ii) TiO_2 rutile particles (Sachtleben R 320 D) are dispersed in part of the SEBS-toluene solution at a 15 vol% concentration using an ultrasonic tip (Fisher Scientific D100 Sonic Dismembrator).

(iii) SEBS-TiO_2 solution is drop casted on a 76.2 × 76.2 mm^2 (3 × 3 in^2) glass slide and let drying for 48 hours to allow evaporation of toluene.

(iv) CB particles (Orion Printex XE 2-B) are dispersed in the remaining SEBS-toluene solution at a 10 vol% concentration and dispersed in a sonic bath over 24 hours.

(v) SEBS-CB solution is painted onto the top and bottom surfaces of the dried dielectric. During the process, two conductive copper tapes are embedded into the liquid electrode

layers to create mechanical connections for the wires linking the sensor to the data acquisition system.

(vi) Resulting multi-layer nanocomposite is let drying for 48 hours to allow evaporation of toluene.

Figure 2(a) shows a schematic representation of the sensor, and Fig. 2(b) is a picture of a single SEC measuring 76.2 × 76.2 mm^2 (3 × 3 in^2). Note that its geometry (e.g., shape and size) can be customized. The resulting sensor combines the advantages of being low cost, highly flexible, mechanically robust, easy to install, and low-powered.

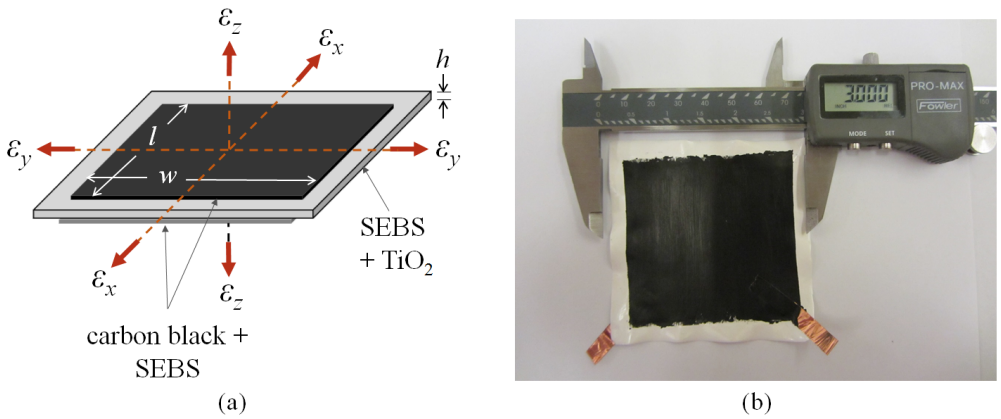

Figure 2: (a) Schematic of SEC with principle axes; and (b) a picture of a single SEC (76.2 × 76.2 mm^2 (3 × 3 in^2)).

2.2. Electromechanical Model

At low measurement frequency (< 1 kHz), the sensor can be approximated as a non-lossy capacitor:

$$C = \frac{e_0 e_r A}{h} \tag{1}$$

where C is the capacitance, $A = w \cdot l$ the surface area of the electrodes of width w and length l, h the thickness of the dielectric (Fig.2(a)), $e_0 = 8.854$ pF/m the vacuum permittivity, and e_r the dimensionless relative permittivity ($e_r \approx 4.2$). A surface strain (e.g., bending, crack) provokes a change in the sensor geometry, which can be measured as a change in capacitance ΔC. Assuming small changes in geometry, Equation (1) can be differentiated to obtain an expression for ΔC:

$$\begin{aligned} \frac{\Delta C}{C} &= \left(\frac{\Delta l}{l} + \frac{\Delta w}{w} - \frac{\Delta h}{h} \right) \\ &= \varepsilon_x + \varepsilon_y - \varepsilon_z \end{aligned} \tag{2}$$

where ε is the sensor strain along the principal axes, as shown in Fig. 2(a). Using Hooke's Law under plane stress assumption, the stress along the z-axis can be written:

$$\varepsilon_z = -\frac{\nu}{1-\nu}(\varepsilon_x + \varepsilon_y) \tag{3}$$

Substituting the expression for ε_z into Equation (2) gives an expression in function of a gauge factor λ:

$$\frac{\Delta C}{C} = \lambda(\varepsilon_x + \varepsilon_y) \tag{4}$$

where

$$\lambda = \frac{\nu}{1-\nu} \tag{5}$$

Note that Equation (4) holds for elastic deformations of the sensor. While the sensing materials is highly elastic, beyond 500% strain [41], it is expected that a fatigue crack would result in highly localized and likely plastic strain, resulting in a more complex formulation relating ΔC to a fatigue crack length. The development of such formulation is out-of-the-scope of this paper.

2.3. Model Validation

The electromechanical model presented above has been validated in Ref. [24, 36] for static and dynamic loads. A typical result is presented here. The sensor was adhered onto the bottom surface of a simply supported aluminum beam, and excited in its bending mode. The excitation history consisted of a displacement-based triangular wave load with increasing frequencies from 0.0167 to 0.40 Hz. Fig. 3 shows the results from the quasi-static load test. The signal of the SEC is converted into strain using Equation (4). A comparison of the measured strain time history versus the strain input at the sensor location is shown in Fig. 3(a). Results show that the SEC is capable of tracking a quasi-static strain history within a given level of resolution. The measurement error is plotted in Fig. 3(b), which confirms an approximate resolution of 25 $\mu\varepsilon$. Lastly, the linearity of the sensor over the measured strain range is illustrated in Fig. 3(c), where the measured capacitance is plotted against the strain input. The slope of the linear fit is the sensitivity S of the sensor. The theoretical sensitivity is $S = \lambda C \approx 1194$ pF$/\varepsilon$, which compares well with the experimental sensitivity $S = 1990$ pF$/\varepsilon$.

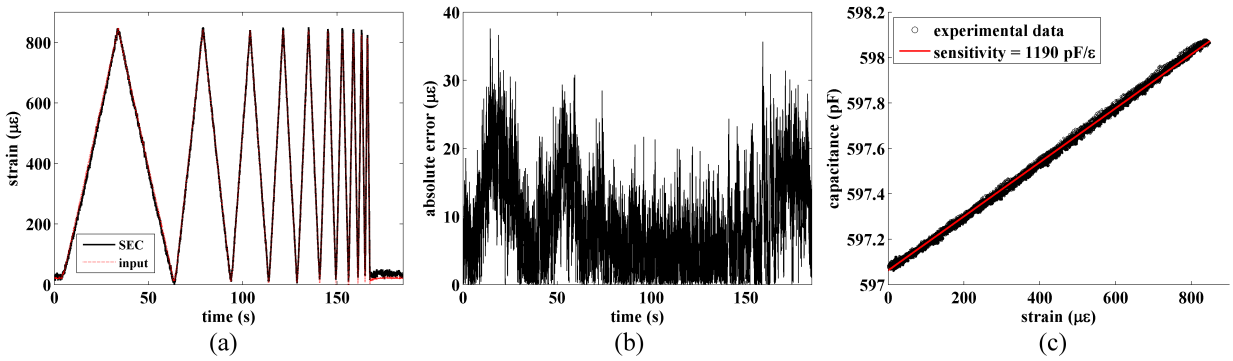

Figure 3: Quasi-static strain test: (a) strain time histories; (b) measurement error; and (c) linearity of the SEC signal.

3. Methodology

Experimental validation is initiated by conducting fatigue crack detection tests. The procedure consists of deploying a single sensor onto a steel specimen subjected to a fatigue load until a fatigue crack is formed. Damage detection is successful if the SEC exhibits a significant change in the recorded strain. Later, validation is conducted for fatigue crack localization. The procedure is similar, but consists of deploying a network of four sensors of which only one is located over the fatigue crack. Damage localization is successful if only one SEC out of the four detects the damage. In this case, one can conclude that the damage is localized under that sensor.

The steel test specimens were prepared and the fatigue crack induced based on the ASTM E647-13a. The specimens used in this study are single edge-notch compact tension (CT) made of A36 steel with an ultimate tensile strengths of 500 MPa (72.5 ksi). The specimens were fabricated with a width of 152 mm (6 in), a thickness of 6.35 mm (0.25 in), and punched holes diameters of 31.8 mm (1.25 in). For the damage detection tests, a sensor of dimensions 76.2×76.2 mm^2 (3×3 in^2) was adhered in the middle of the specimen surface (Fig. 5(a)). Smaller SECs of dimensions 38.1×38.1 mm^2 (1.5×1.5 in^2) were used in the damage localization tests to accommodate all sensors (Fig. 10(a)). To help the growth of the fatigue crack, the specimens were cut 0.31 in at the notch using the recommended minimum value in ASTM E647-13a. Figure 4(a) shows the details of the compact specimen from ASTM E647-13a, and Fig. 4(b) shows the dimensions used in the experiment.

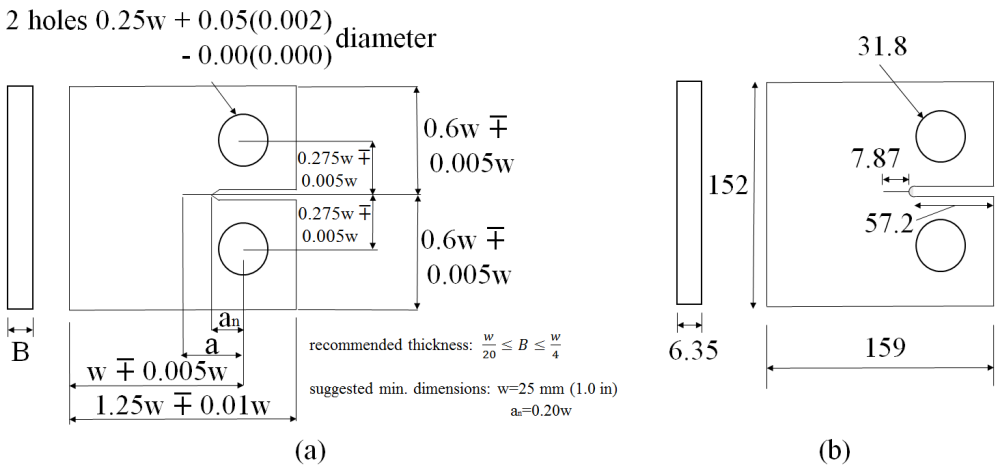

Figure 4: (a) Details of a standard compact specimen for testing of fatigue crack growth (adapted from ASTM E647-13a); and (b) dimensions (mm) of the test specimens.

The SECs were installed using the following methodology. Each test specimen was sanded at the sensor location and painted with a primer. The sensors were then deployed onto the specimen using a thin layer of an off-the-shelf epoxy (JB Kwik) (Fig. 5(b)). The test specimens were gripped by a clevis and pin assembly attached to the top and bottom holes as shown in Fig. 5(a). Data from the SEC were acquired using an off-the-shelf capacitance data acquisition system (DAQ - ACAM PCap01). To reduce electromagnetic noise, the test specimens and the DAQ were grounded, and the DAQ was enclosed in a Faraday cage. The utilization of shielded cable may further reduce noise. Note that a dedicated DAQ is currently being developed to digitize the signal directly next to the SEC to further reduce noise in the measurements. Also, the SEC has a linear dependence on temperature and humidity. In practical applications, these environmental effects can be minimized or eliminated by comparing changes in capacitance over small periods of time (during which both the temperature and humidity are approximately constant), by adjusting the signal with respect to the measured environmental states, or by connecting SECs in Wheatstone bridge configurations. During the tests, the temperature of the SECs and humidity of the laboratory were monitored, and no significant changes were noted over the length of each experiment.

A computer-controlled MTS 810 electric servo-hydraulic 24.5 kN (5.5 kips) stand was used to load the specimens at frequency of 20 Hz. The laboratory setup is shown in Fig. 5(c). Tests were conducted in a tension-tension mode under a maximum and minimum loads of 29 kN (6.5 kips) and 2.9 kN (0.65 kips), respectively. Note that this load intensity is higher than recommended by the ASTM E647-13a in order to accelerate the crack growth, which may cause wider crack widths than typical. Nevertheless, the objective of the test is to investigate changes in the signal of the sensor with respect to the formation of a fatigue

crack for a given width.

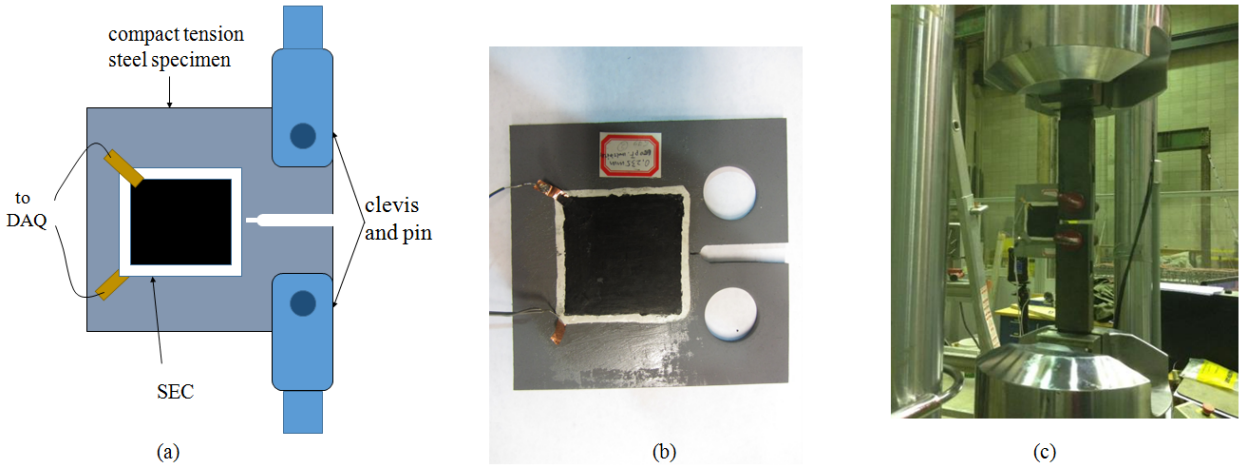

Figure 5: (a) Schematic of the laboratory setup (damage detection test); (b) picture of the prepared test specimen with an SEC; and (c) picture of the laboratory setup.

The test specimens were visually inspected during tests to monitor crack development, and pictures were taken using a Canon T2i DSLR camera 18.0-megapixel. These pictures were post-processed using a pixel count to determine the crack length and width using the known width of the clevis as a reference. Fig. 6 shows the evolution of a fatigue crack for a typical test. The crack pattern is first formed onto the specimen surface (Fig. 6(a)) and time of visual observation recorded. At this stage, it is uncertain whether the crack is running through the sample or is only on the surface coating. The crack then quickly grows along its length (Fig. 6(b)), and the MTS is stopped. Fig. 6(c) represents the additional growth of the fatigue crack the occurs during the delay between the observation of crack growth (Fig. 6(b)) and the actual stop of the MTS. Note that given the rapidity of the crack growth, it was not always possible to take a timely and clear picture of the crack immediately after initiation. For this reason, sensor data is compared across tests using the crack size measured from the pictures taken when the MTS was stopped and its load completely released.

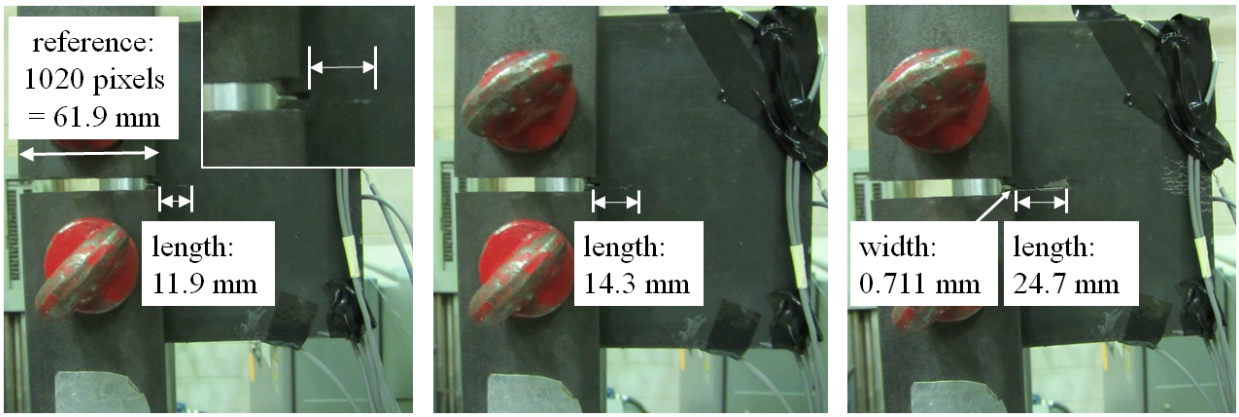

Figure 6: Typical fatigue crack growth during tests: (a) initiation (blowup of the crack at the top right corner); (b) crack growth; and (c) crack expended at MTS stop.

4. Experimental Results

4.1. Damage Detection

A series of tests was conducted on specimens equipped with a single SEC to study the capacity of the sensor to detect damage. Figure 7 shows the time series measurements of the SECs for all three tests. A low-pass filter was used to smoothen data. The vertical dashed line in each plot indicates the time at which the fatigue crack was visually observable (Fig. 6(a)). Time series data from Fig. 7 show that the formation of the fatigue crack is visually observable in the capacitance signal, featured by a step increase in the time series data before the signal plateaus because of the test termination. This step increase is more significant in test 3 (Fig. 7(c)), due to the formation of a larger crack as listed in Table 1.

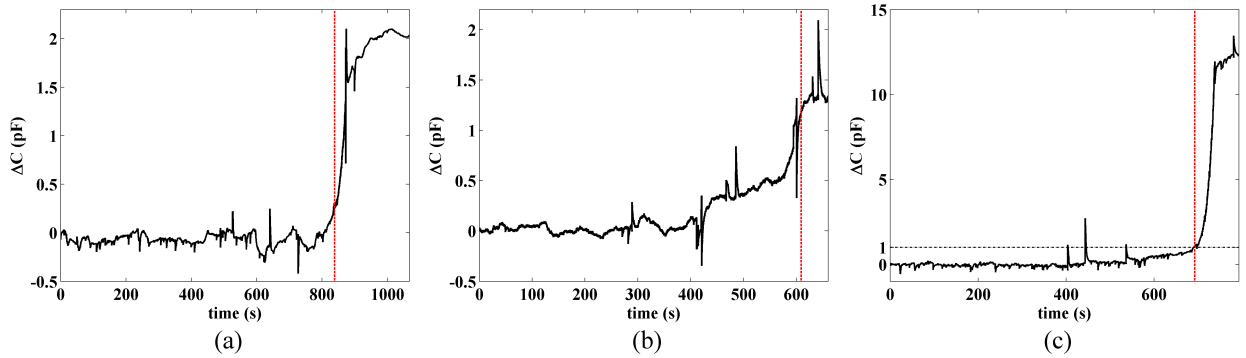

Figure 7: Time history versus capacitance for (a) test 1; (b) test 2; and (c) test 3. The vertical dashed line denotes the time at which the fatigue crack was visually observable.

Table 1: Fatigue crack sizes for damage detection tests.

	crack length mm (in)	crack width mm (in)
test 1	29.9 (1.176)	0.254 (0.010)
test 2	27.2 (1.069)	0.305 (0.012)
test 3	32.5 (1.279)	0.711 (0.028)
average	29.8 (1.175)	0.432 (0.017)

Figure 8 shows the picture of the specimens taken after pausing of the MTS. Table 1 reports the dimensions of cracks and width of clevis in both pixels and inches. The results show that the smallest detectable crack length and width are 27.2 mm (1.069 in) and 0.254 mm (0.010 in), respectively, and the average detectable crack length and width are 29.8 mm (1.175 in) and 0.432 mm (0.017 in), respectively. Nevertheless, the SEC signals already exhibit a significant change in the signal at the time of visual observation of crack initiation. This indicates that the smart sensing skin may possibly detect smaller crack sizes.

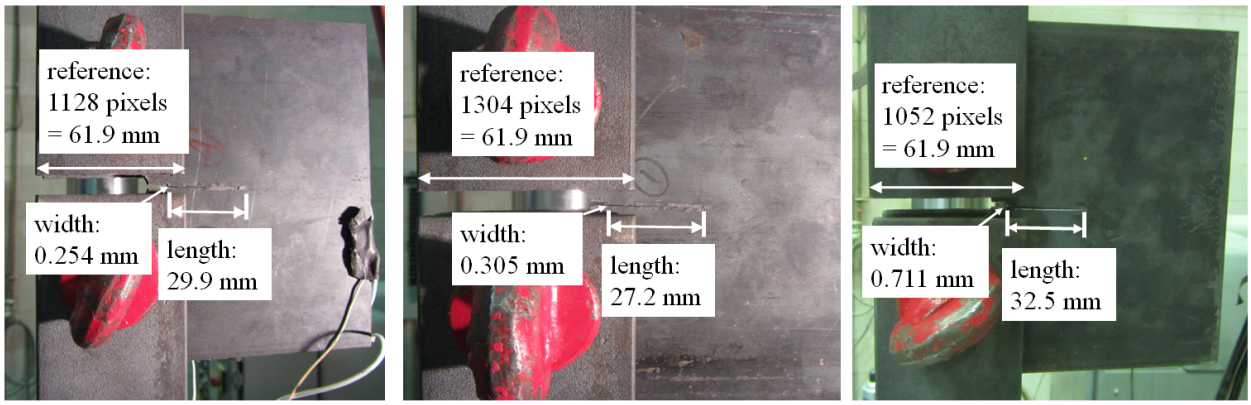

Figure 8: Pictures of cracked specimens at the plateau: (a) test 1; (b) test 2; and (c) test 3.

Fig. 9 is a plot of the corresponding measured strain $\varepsilon_x + \varepsilon_y$ using Equation (4) and a gauge factor $\lambda = 2$, for the last 300 seconds of each test. As discussed previously, because the fatigue crack results in a localized and likely plastic deformation of the sensor, the strain level does not correspond directly to the crack size, but gives instead an order of crack severity.

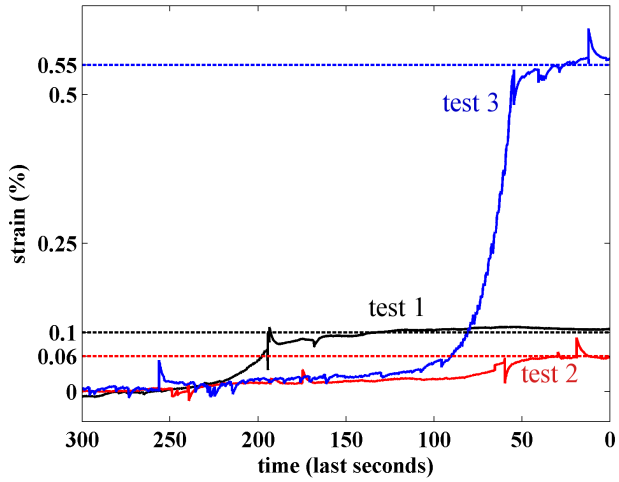

Figure 9: Strain time histories for the last 300 seconds.

4.2. Damage Localization

A second series of tests was conducted to evaluate the capacity of the SEC at localizing a fatigue cracks. Fig. 10(a) is a schematic of the laboratory setup. Four sensors were used in a network configuration. Fig. 10(b) shows the numbering scheme used in the experiment. Using results from the damage detection tests, a crack length of approximately 25.4 mm (1 in) was expected, therefore running under SEC 1 only.

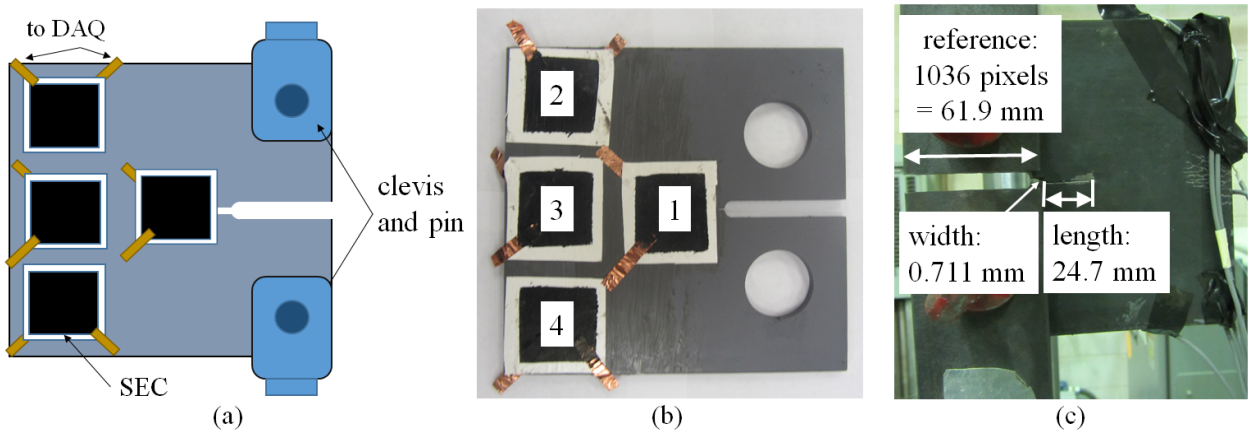

Figure 10: (a) Schematic of the laboratory setup (damage localization test); (b) sensor placement; and (c) picture of test results.

The picture of a typical test result is shown in Fig. 10(c), with a fatigue crack of length and width of 24.7 mm (0.974 in) and 0.711 mm (0.028 in), respectively. Fig. 11 is a plot of the time series of all SECs showing the change in capacitance (Fig. 11(a)) and the corresponding strain using Equation (4) (Fig. 11(b)). The vertical dashed line in each plot indicates the

time at which the fatigue crack was visually observable. Note that each SEC has a different initial capacitance C, resulting in a different scaling of each signal in the transformation to strain data. Results show that only SEC 1 has a significant change in data when the crack is formed, which enables both detection and localization (there is a crack, and it is located only under SEC 1). The change in capacitance has levels comparable to results from the damage detection tests (Fig. 7) for a crack size similar to test 2 in length and similar to test 3 in width. The corresponding level of strain is higher given that the initial capacitance C is approximately halved from using smaller sensors having approximately half the area compared with the sensors used for the damage detection tests.

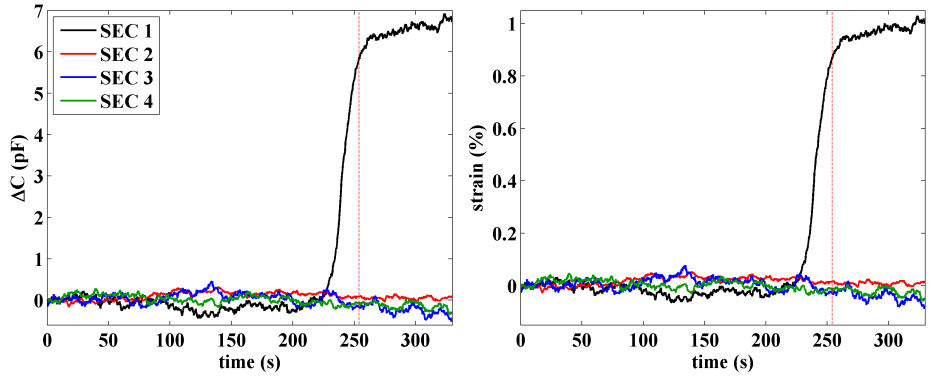

Figure 11: Time histories for damage detection test: (a) change in capacitance; and (b) measured strain. The vertical dashed line denotes the time at which the fatigue crack was visually observable.

5. Conclusion

In this paper, the capability of a novel sensor, termed SEC, at detecting and localizing fatigue cracks was investigated. The SEC is a flexible large area electronics capable of covering very large areas at low cost. It is analogous to sensing skin, in the sense that it has the potential to monitor local deformations over a global area. Such feature makes it an ideal sensing solution for detecting and localizing local damages, such as fatigue cracks.

The background on the SEC was presented, which included the sensing materials, the electromechanical model, and a validation of the sensing principle. After, the testing methodology was discussed. Two test types have been conducted. The first one consisted of validating the damage detection capability by deploying a single sensor on a steel specimen subjected to a fatigue load. Time series measurements from a sensor was correlated with visual observations and specimen pictures. A significant change in the measured signal occurred when the fatigue crack formed, which showed that damage was successfully detected. The smallest detectable crack length and width are 27.2 mm (1.069 in) and 0.254

mm (0.010 in), respectively, and the average detectable crack length and width are 29.8 mm (1.175 in) and 0.432 mm (0.017 in), respectively.

After this validation, a second series of tests was conducted to determine whether a network of SECs could be used also to localize damage. A similar methodology was used, but this time using four SECs. Time series results showed that only the SEC located over the formed fatigue crack detected the damage via a significant changed in its capacitance measurements. This validated that a network of SECs could be used to localize a fatigue crack.

It follows that the novel sensor demonstrated a promising capability to detect and localize fatigue cracks when it is deployed in a network configuration, and at an early stage. By being applicable to large surfaces, the sensor has a substantial advantage over conventional resistive strain gauges that are too small to successfully locate a new crack within acceptable probabilities. Future research enabling field applications include the development of a dedicated data acquisition system and energy harvesting capability for autonomous and continuous sensing, as well as algorithms to transform the sensor signal into damage indices.

Acknowledgments

This work is supported by grant #RT 454-494 from the Iowa Department of Transportation. Their support is gratefully acknowledged. The authors are also indebted to Ping Lu from the Iowa Department of Transportation and Loren Risch from the Kansas Department of Transportation.

References

[1] Stephen John Maddox. *Fatigue strength of welded structures*. Woodhead publishing, 1991.

[2] T.M. Roberts and M. Talebzadeh. Acoustic emission monitoring of fatigue crack propagation. *Journal of Constructional Steel Research*, 59(6):695–712, 2003.

[3] S.I. Rokhlin and J.-Y. Kim. In situ ultrasonic monitoring of surface fatigue crack initiation and growth from surface cavity. *International journal of fatigue*, 25(1):41–49, 2003.

[4] M. Huang, L. Jiang, P. K. Liaw, C. R. Brooks, R. Seeley, and D. L. Klarstrom. Using acoustic emission in fatigue and fracture materials research. *Journal of The Minerals, Metals & Materials Society*, 50(11):1–14, 1998.

[5] W.J. Staszewski, B.C. Lee, and R. Traynor. Fatigue crack detection in metallic structures with lamb waves and 3d laser vibrometry. *Measurement Science and Technology*, 18(3):727, 2007.

[6] G. Zenzinger, J. Bamberg, W. Satzger, and V. Carl. Thermographic crack detection by eddy current excitation. *Nondestructive Testing and Evaluation*, 22(2-3):101–111, 2007.

[7] N. Yusa, L. Janousek, M. Rebican, Zhenmao C., Kenzo M., N. Chigusa, and H. Ito. Detection of embedded fatigue cracks in inconel weld overlay and the evaluation of the minimum thickness of the weld overlay using eddy current testing. *Nuclear Engineering and Design*, 236(18):1852–1859, 2006.

[8] J. Vrana, M. Goldammer, J. Baumann, M. Rothenfusser, W. Arnold, D.O. Thompson, and D.E

Chimenti. Mechanisms and models for crack detection with induction thermography. In *AIP conference Proceedings*, volume 975, page 475, 2008.

[9] J. Renshaw, J.C. Chen, S.D. Holland, and R.B. Thompson. The sources of heat generation in vibrothermography. *NDT & E International*, 44(8):736–739, 2011.

[10] Y. Zhang. In situ fatigue crack detection using piezoelectric paint sensor. *Journal of Intelligent Material Systems and Structures*, 17(10):843–852, 2006.

[11] L. Yu, V. Giurgiutiu, P. Ziehl, D. Ozevin, and P. Pollock. Steel bridge fatigue crack detection with piezoelectric wafer active sensors. In *SPIE Smart Structures and Materials+ Nondestructive Evaluation and Health Monitoring*, pages 76471Y–76471Y. International Society for Optics and Photonics, 2010.

[12] M. Gresil, L. Yu, Y. Shen, and V. Giurgiutiu. Predictive model of fatigue crack detection in thick bridge steel structures with piezoelectric wafer active sensors. *Smart Structures and Systems*, 12(2):1738–1584, 2013.

[13] J.-B. Ihn and F.-K. Chang. Detection and monitoring of hidden fatigue crack growth using a built-in piezoelectric sensor/actuator network: Ii. validation using riveted joints and repair patches. *Smart Materials and Structures*, 13(3):621, 2004.

[14] A.L. Gama and S.R.K. Morikawa. Monitoring fatigue crack growth in compact tension specimens using piezoelectric sensors. *Experimental Mechanics*, 48(2):247–252, 2008.

[15] H. Tsuda, J.-R. Lee, and Y. Guan. Fatigue crack propagation monitoring of stainless steel using fiber bragg grating ultrasound sensors. *Smart materials and structures*, 15(5):1429, 2006.

[16] H. Tsuda, J.-R. Lee, Y. Guan, and J. Takatsubo. Investigation of fatigue crack in stainless steel using a mobile fiber bragg grating ultrasonic sensor. *Optical Fiber Technology*, 13(3):209–214, 2007.

[17] D.C. Lee, J.J. Lee, I.B. Kwon, and D.C. Seo. Monitoring of fatigue damage of composite structures by using embedded intensity-based optical fiber sensors. *Smart materials and structures*, 10(2):285, 2001.

[18] J.M. López-Higuera, L. Rodriguez Cobo, A.o Quintela Incera, and A. Cobo. Fiber optic sensors in structural health monitoring. *Lightwave Technology, Journal of*, 29(4):587–608, 2011.

[19] I. Mohammad and H. Huang. Monitoring fatigue crack growth and opening using antenna sensors. *Smart Materials and Structures*, 19(5):055023, 2010.

[20] X. Yi, C. Cho, J. Cooper, Y. Wang, M.M. Tentzeris, and R.T. Leon. Passive wireless antenna sensor for strain and crack sensing—electromagnetic modeling, simulation, and testing. *Smart Materials and Structures*, 22(8):085009, 2013.

[21] M.E. Ibrahim and R.J. Ditchburn. Monitoring of fatigue cracks using permanently-mounted conformable eddy-current sensors. In *Materials Forum*, volume 33, pages 336–343, 2009.

[22] D. Roach. Real time crack detection using mountable comparative vacuum monitoring sensors. *Smart structures and systems*, 5(4):317–328, 2009.

[23] S. Laflamme, M. Kollosche, J.J. Connor, and G. Kofod. Robust flexible capacitive surface sensor for structural health monitoring applications. *Journal of Engineering Mechanics*, 139(7):879–885, 2012.

[24] S. Laflamme, H.S. Saleem, B.K Vasan, R.L. Geiger, D. Chen, M.R. Kessler, and K. Rajan. Soft elastomeric capacitor network for strain sensing over large surfaces. *IEEE/ASME Transactions on Mechatronics*, 18(6):1647–1654, 2013.

[25] I. Kang, M.J. Schulz, J.H. Kim, V. Shanov, and D. Shi. A carbon nanotube strain sensor for structural health monitoring. *Smart Materials and Structures*, 15(3):737, 2006.

[26] K.J. Loh, T.C. Hou, J.P. Lynch, and N.A. Kotov. Carbon nanotube sensing skins for spatial strain and impact damage identification. *Journal of Nondestructive Evaluation*, 28(1):9–25, 2009.

[27] L. Gao, E.T. Thostenson, Z. Zhang, J.-H. Byun, and T.-W. Chou. Damage monitoring in fiber-reinforced composites under fatigue loading using carbon nanotube networks. *Philosophical Magazine*, 90(31-32):4085–4099, 2010.

[28] R.K. Srivastava, V.S.M. Vemuru, Y. Zeng, R. Vajtai, S. Nagarajaiah, P.M. Ajayan, and A. Srivastava. The strain sensing and thermal–mechanical behavior of flexible multi-walled carbon nanotube/polystyrene composite films. *Carbon*, 49(12):3928 – 3936, 2011.

[29] Y. Hu, W.S.A. Rieutort-Louis, J. Sanz-Robinson, L. Huang, B. Glisic, J.C. Sturm, S. Wagner, and N. Verma. Large-scale sensing system combining large-area electronics and cmos ics for structural-health monitoring. *Solid-State Circuits, IEEE Journal of*, 49(2):513–523, 2014.

[30] S.T. Tung, Y. Yao, and B. Glisic. Sensing sheet: the sensitivity of thin-film full-bridge strain sensors for crack detection and characterization. *Measurement Science and Technology*, 25(7):075602, 2014.

[31] H.P. Hong, K.H. Jung, N.K. Min, Y.H. Rhee, and C.W. Park. A highly fast capacitive-type humidity sensor using percolating carbon nanotube films as a porous electrode material. In *Sensors, 2012 IEEE*, pages 1–4, Oct 2012.

[32] D.J. Lipomi, M. Vosgueritchian, B.C.K. Tee, S.L. Hellstrom, J.A. Lee, C.H. Fox, and Z. Bao. Skin-like pressure and strain sensors based on transparent elastic films of carbon nanotubes. *Nature nanotechnology*, 6(12):788–792, 2011.

[33] K.I. Arshak, D. McDonagh, and M.A. Durcan. Development of new capacitive strain sensors based on thick film polymer and cermet technologies. *Sensors and Actuators A: Physical*, 79(2):102 – 114, 2000.

[34] M. Suster, Jun G., N. Chaimanonart, W.H. Ko, and D.J. Young. A high-performance mems capacitive strain sensing system. *Microelectromechanical Systems, Journal of*, 15(5):1069–1077, Oct 2006.

[35] J.A. Dobrzynska and M.A.M. Gijs. Polymer-based flexible capacitive sensor for three-axial force measurements. *Journal of Micromechanics and Microengineering*, 23(1):015009, 2013.

[36] F. Ubertini, S. Laflamme, H. Ceylan, A.L. Materazzi, G. Cerni, H. Saleem, A. D'Alessandro, and A. Corradini. Novel nanocomposite technologies for dynamic monitoring of structures: a comparison between cement-based embeddable and soft elastomeric surface sensors. *Smart Materials and Structures*, 23(4):045023, 2014.

[37] S. Laflamme, F. Ubertini, H. Saleem, A. D'Alessandro, A. Downey, H.l Ceylan, and A.L. Materazzi. Dynamic characterization of a soft elastomeric capacitor for structural health monitoring. *Journal of Structural Engineering*, 2014.

[38] Ryuichiro Yoda. Elastomers for biomedical applications. *Journal of Biomaterials Science, Polymer Edition*, 9(6):561–626, 1998.

[39] H. Stoyanov, M. Kollosche, D. N. McCarthy, and G. Kofod. Molecular composites with enhanced energy density for electroactive polymers. *Journal of Material Chemistry*, 20:7558–7564, 2010.

[40] Jan-Chan Huang. Carbon black filled conducting polymers and polymer blends. *Advances in Polymer Technology*, 21(4):299–313, 2002.

[41] H. Saleem, M. Thunga, M. Kollosche, M.R. Kessler, and S. Laflamme. Interfacial treatment effects on behavior of soft nano-composites for highly stretchable dielectrics. *Polymer*, 55(17):4531–4537, 2014.